PERGAMON

Pattern Recognition 33 (2000) 1383–1393

PATTERN RECOGNITION
THE JOURNAL OF THE PATTERN RECOGNITION SOCIETY

www.elsevier.com/locate/patcog

Model-based segmentation of nuclei

Ge Cong*, Bahram Parvin

Information and Computing Science Division, Lawrence Berkeley National Laboratory, MS 50B-2239, 1 Cyclotron Road, Berkeley, CA 94720, USA

Received 16 December 1998; accepted 29 April 1999

Abstract

A new approach for the segmentation of nuclei observed with an epi-fluorescence microscope is presented. The proposed technique is model based and uses local feature activities in the form of step-edge segments, roof-edge segments, and concave corners to construct a set of initial hypotheses. These local feature activities are extracted using either local or global operators and corresponding hypotheses are expressed as hyperquadrics. A neighborhood function is defined over these features to initiate the grouping process. The search space is expressed as an assignment matrix with an appropriate cost function to ensure local and neighborhood consistency. Each possible configuration of nucleus defines a path and the path with least overall error is selected for final segmentation. The system is interactive to allow rapid localization of large numbers of nuclei. The operator then eliminates a small number of false alarms and errors in the segmentation process. © 2000 Pattern Recognition Society. Published by Elsevier Science Ltd. All rights reserved.

Keywords: Segmentation; Grouping; Hyperquadric; Medical image processing; Shape recovery

1. Introduction

Automatic delineation of cell nuclei is an important step in mapping functional activities into structural components in cell biology. This paper examines delineation of individual nucleus that are observed with an epi-fluorescence microscope. The nuclei that we are dealing with are in mammary cells. These cells cover the capillaries that carry milk in the breast tissues. The nuclei of interest reside in a thin layer that surround a particular type of capillary in the tissue. The intent is to build the necessary computational tools for large-scale population studies and hypothesis testing. These nuclei may be clumped together, thus, making quick delineation infeasible. At present stage, we are working on 2D crossing-section images of the tissue which are obtained by focusing the optical system at specific locations along the z-axis. Thus, we can assume that the nuclei abut but do not overlap each other. An example is shown in Fig. 1(a). Previous efforts in this area have been focused on thresholding, local geometries, and morphological operators for known cell size [1,2]. Others have focused on an *optimal cut path* that minimizes a cost function in the absence of shape, size, or other information [3–7].

In this paper, we propose a new approach that utilizes both step-edge and roof-edge boundaries to partition a clump of nuclei in a way that is globally consistent. In this context, images are binarized and boundaries – corresponding to step edges – are recovered. Next, concave corners are extracted from polygonal approximation of the initial boundary segments. These corners provide possible cues to where two adjacent nuclei may come together. Thresholding separates big clumps consisting of several nuclei squeezed together. The boundaries between every two adjacent nuclei inside one clump are not detected by thresholding since they have higher intensities, as shown in Fig. 1(b) and (c). Thus, crease segments are detected [8–11] which provide additional boundary conditions for the grouping process, as shown in Fig. 1(d). These crease segments correspond to trough edges and are treated as common boundaries between adjacent nuclei. False creases may be extracted in the process.

* Corresponding author. Tel.: +510-486-4158; fax: +510-486-6363.

E-mail address: gcong@george.lbl.gov (G. Cong).

PII: S0031-3203(99)00119-3

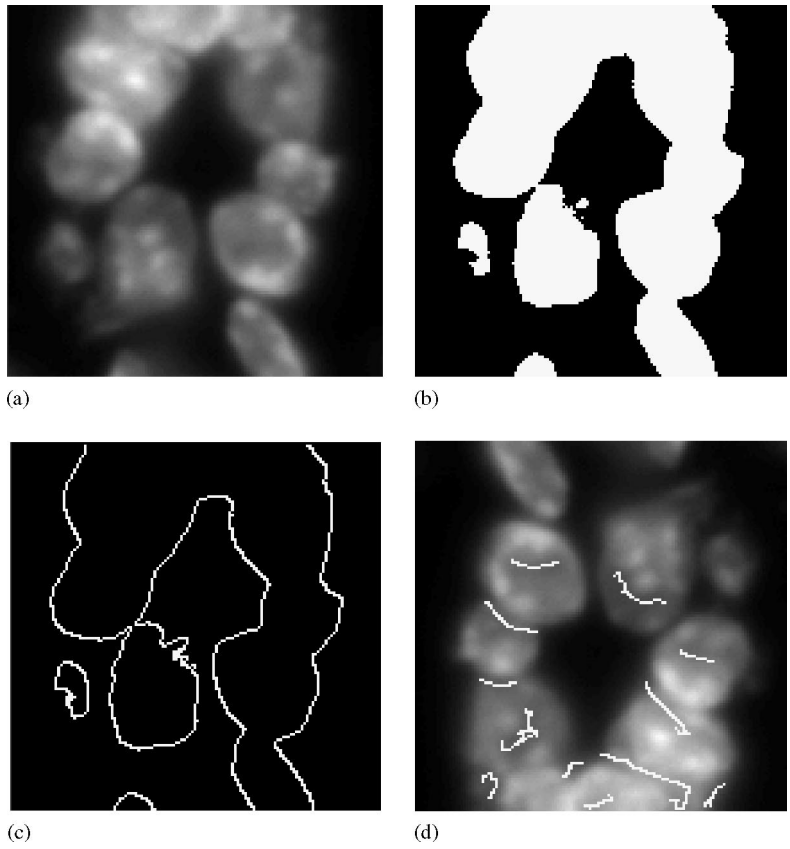

Fig. 1. An example of nuclei with the results of global and local operations: (a) original image; (b) threshold image; (c) boundary objects; and (d) local troughs.

However, since our algorithm need not use all the segments provided, false crease segments can be discarded in the grouping stage in favor of the global optimization. A unique feature of our system is in hyperquadric representation of each hypothesis and the use of this representation for global consistency. The main advantage of such a parameterized representation – as opposed to polygonal representation – is better stability in shape description from partial information. In this fashion, each step-edge boundary segment belongs to one and only one nucleus while each roof-edge boundary segment is shared by two and only two nuclei. These initial hypotheses and their localized inter-relationship provides the basis for search in the grouping step. This is expressed in terms of an adequate cost function and minimized through dynamic programming. The final result of this computational step is then shown to a user for verification and elimination of false alarms.

In the next section, we will briefly review each step of the representation process and parameterization of each hypothesis in terms of hyperquadric. This will be followed by the details of the grouping protocol, results on real data, and concluding remarks.

2. Representation

The initial step of the computational process is to collect sufficient cues from local feature activities so that a set of hypotheses – not all of them correct – can be constructed for consistent grouping. These initial steps include thresholding, detection of concave points from boundary segments, extraction of crease segments from images, and hyperquadric representation of each possible hypothesis.

2.1. Thresholding

Binary thresholding extracts the clump patterns from the original image. The corresponding threshold can be obtained through analysis of the intensity histogram or contrast histogram. As shown in Fig. 2, since background

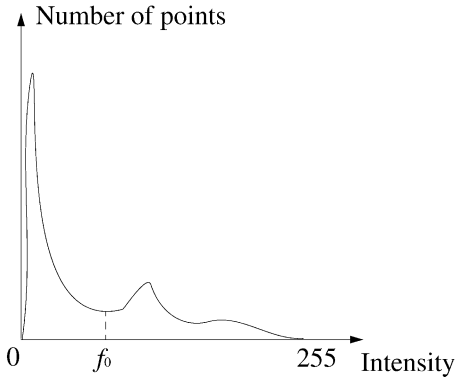

Fig. 2. Thresholding.

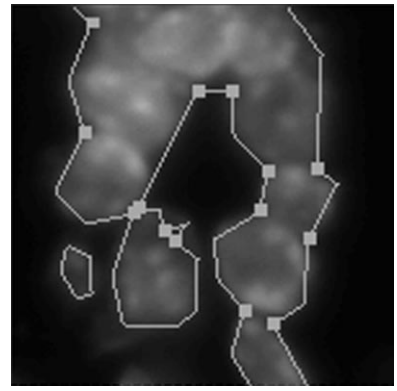

Fig. 3. Detection of concave corners.

always corresponds to the first peak in the intensity histogram, intensity analysis select the first valley following this peak as the threshold. In the contrast analysis, optimum threshold corresponds to the peak in the contrast histogram which is the accumulation of local contrast at each edge point. Thresholding is a valid approach for fluorescence images because of absence of any shading artifact.

2.2. Polygonal approximation

The next step is to partition the clump silhouettes into segments that are partial nucleus boundaries. Often the location on the boundary between two adjacent nuclei is signaled by a concave point, thus, a reliable corner detector is needed. These corners are localized by the concave vertices of the polygonal approximation of the original contours [1,12] and the concavity is determined by the turning angle between adjacent line segments. The arcs of the clump boundaries between every two adjacent corners are defined as the "boundary segments". Since polygonal approximation just selects some "feature points" from the original curve as new vertices, all the corners are guaranteed to be on the original boundaries. An example of this step of the process is shown in Fig. 3.

2.3. Detection of crease boundaries

This step detect the common boundaries between every two squeezed nuclei in one clump which can be modeled as crease features. In grey images, crease points can be defined as local extremes of the principal curvature along the principal direction [8–11]. It is well known that due to noise, scale, finite differential operators, and thresholds, it is very difficult to detect complete creases as shown in Fig. 1(d). Images are enhanced through a variation of nonlinear diffusion [13] to improve localization of crease points. The principal curvature k is then computed as the solution of the following Eq. [14]

$$(EG - F^2)k^2 - (EN + GL - 2FM)k + (LN - M^2) = 0 \quad (1)$$

Where E, F, G, L, M, N are the *first* and *second* fundamental forms:

$$E = 1 + f_x^2,$$

$$F = f_x f_y,$$

$$G = 1 + f_y^2,$$

$$L = f_{xx},$$

$$M = f_{xy},$$

$$N = f_{yy}.$$

The principal direction $(\mathrm{d}x : \mathrm{d}y)$ is given by the following Eq. [14]:

$$(EM - LF)\,\mathrm{d}x^2 + (EN - LG)\,\mathrm{d}x\,\mathrm{d}y + (FN - MG)\,\mathrm{d}y^2 = 0. \quad (2)$$

Crease points are detected and linked to form "crease segments" as shown in Fig. 1(d).

2.4. Hyperquadric model

A brief introduction to hyperquadric fitting is included. A more detailed description can be found in [15–17]. A 2D hyperquadric is a closed curve defined by:

$$\sum_{i=1}^{N} |A_i x + B_i y + C_i|^{\gamma_i} = 1. \quad (3)$$

Since $\gamma_i > 0$, Eq. (3) implies that

$$|A_i x + B_i y + C_i| \leqslant 1, \quad \forall i = 1, 2, \ldots, N, \quad (4)$$

which corresponds to a pair of parallel line segments for each i. These line segments define a convex polytope (for large γ) within which the hyperquadric is constrained to lie. This representation is valid across a broad range of shapes which need not be symmetric. The parameters A_i and B_i determine the slopes of the bounding lines and, along with C_i, the distance between them. γ_i determines the "squareness" of the shape. Hyperquadric can model both convex and concave shapes, thus, we do not assume that the nuclei is convex in our approach.

2.4.1. Fitting problem

Assume that m data points $p_j = (x_j, y_j), j = 1, 2, \ldots, m$ from n segments ($m = \sum_{i=1}^{n} m_i$) are given. The cost function is defined as

$$\varepsilon^2 = \sum_{j=1}^{m} \frac{1}{\|\nabla F_j(p_j)\|^2}(1 - F_j(p_j))^2 + \lambda \sum_{i=1}^{N} Q_i, \tag{5}$$

where $F_j(p_j) = \sum_{i=1}^{N} |A_i x_j + B_i y_j + C_i|^{\gamma_i}$, ∇ is the gradient operator, λ is the regularization parameter and Q_i is the constraint term [17]. The parameters A_i, B_i, C_i, γ_i are calculated by minimizing ε using the Levenberg–Marquard non-linear optimization method [18] from a suitable initial guess [17]. Several examples of hyperquadric fitting to an initial set of partial segments are shown in Fig. 4.

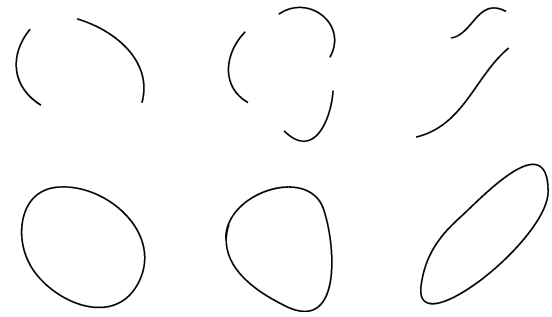

Fig. 4. Fitting results for hyperquadrics.

3. Grouping for nuclei

Let each clump be represented by n_b boundary segments $b_i, i = 1, \ldots, n_b$ and n_c crease segments c_i, $i = 1, \ldots, n_c$. We assume that there are at most n_b nuclei in the clump because each nucleus should have at least one boundary segment detected to indicate its existence. The nucleus Φ_i correspondent to the index of b_i is defined as a set of boundary and crease segments belonging to the ith nucleus. Note that Φ_i does not necessarily include b_i and may be empty. All the segments in a certain Φ_i is fitted by the hyperquadric as the actual shape of the nucleus. To delineate the nuclei in one clump, we need to find the assignment of all $b_i, i = 1, \ldots, n_b$ and c_i, $i = 1, \ldots, n_c$ to $\Phi_i, i = 1, \ldots, n_b$. According to their characters, each b_i belongs to one and only one Φ_i while each c_i belongs to two different nuclei (common boundary) or not a single nucleus (false crease). This is called the consistence criterion. Thus, two or more boundary segments may be assigned to the same Φ_i while some other Φ_i are unfilled.

To assign the segments, we define a new set $\tilde{\Phi}_i$ for each Φ_i such that $\Phi_i \subseteq \tilde{\Phi}_i$. It is assumed that detecting $\tilde{\Phi}_i$ is trivial and $\tilde{\Phi}_i$ contains all the segments that have certain possibilities to be part of the ith nucleus. Computing Φ_i from $\tilde{\Phi}_i$ is in fact subject to local, adjacency, and global constraint. It is under-constrained and the solution is not unique. Each possible solution is measured by the "goodness criteria" proposed in Section 3.3 and the one with minimum cost determines the segmentation.

3.1. Neighborhood box

A neighborhood box, which is defined over a region for each b_i, is used to construct the $\tilde{\Phi}_i$, as shown in Fig. 5. Suppose that p_1 and p_2 are the end points of b_i and r is the line segment connecting them with $l = \|r\|$ as the length. The neighborhood box is then defined as the combination of a square that extends r and the region enclosed by b_i. The length of the square edge is a pre-set number L unless $l > L$ where the length is set to l.

Any segment $b_j, j = 1, \ldots, n_b$ or $c_j, j = 1, \ldots, n_c$ that resides in the neighborhood box is included in $\tilde{\Phi}_i$. When L is properly selected, all the boundary and crease segments of Φ_i are guaranteed to be in the neighborhood box, thus, $\Phi_i \subseteq \tilde{\Phi}_i$.

3.2. Search strategy

Our next step is to compute Φ_i from $\tilde{\Phi}_i$ subjected to the consistence criterion. Since every segment in $\tilde{\Phi}_i$ has some possibility to be in Φ_i, the solution is not unique. However, the construction of $\tilde{\Phi}_i$ reduces greatly the searching space. The optimal segmentation is computed by measuring different solutions based on global evolution criteria.

The key data structure in our approach is the *Assignment Matrix* $\mathcal{M}$. Each row of $\mathcal{M}$ indicates a possible nucleus. For the clump under investigation, we can construct up to n_b nuclei. Thus, $\mathcal{M}$ has n_b rows. Each column of $\mathcal{M}$ indicates a boundary or crease segment. Since each crease may be shared by two nuclei, we assign two columns for it. Thus, $\mathcal{M}$ has $n_b + 2n_c$ columns. Let

$$s_j = b_j, 1 \leqslant j \leqslant n_b,$$

$$s_{n_b+2j-1} = s_{n_b+2j} = c_j, \quad 1 \leqslant j \leqslant n_c, \tag{6}$$

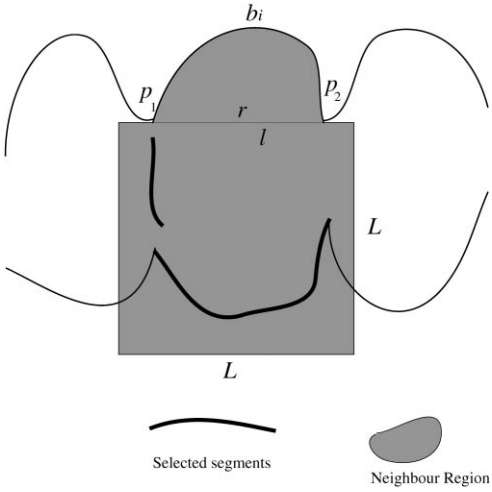

Fig. 5. Neighborhood function.

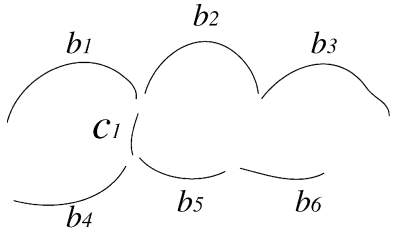

Fig. 6. An example of boundary and crease segments.

	s_1	s_2	s_3	s_4	s_5	s_6	s_7	s_8
nucleus 1	1	0	0	1	1	0	1	1
nucleus 2	0	1	0	0	1	1	1	1
nuclues 3	0	0	1	0	0	1	0	0
nucleus 4	1	0	0	1	0	0	1	1
nucleus 5	0	1	0	0	1	0	1	1
nucleus 6	0	0	1	0	0	1	0	0

Path I
Path II

Fig. 7. Assignment matrix for features of Fig. 6.

$\mathcal{M}$ is determined by

$$m_{ij} = \begin{cases} 1 & \text{if } s_j \in \tilde{\Phi}_i, \\ 0 & \text{otherwise.} \end{cases} \tag{7}$$

An example for construction of $\mathcal{M}$ for feature segments of Fig. 6 is shown in Fig. 7, where we assume that

$$\tilde{\Phi}_1 = \{b_1, c_1, b_4, b_5\},$$

$$\Phi_2 = \{b_2, c_1, b_5, b_6\},$$

$$\tilde{\Phi}_3 = \{b_3, b_6\},$$

$$\tilde{\Phi}_4 = \{b_4, c_1, b_1\},$$

$$\tilde{\Phi}_5 = \{b_5, c_1, b_2\},$$

$$\tilde{\Phi}_6 = \{b_6, b_3\}. \tag{8}$$

The ith row of $\mathcal{M}$ represents all possible segments that may be part of a nucleus. The jth column of $\mathcal{M}$ indicates all possible nuclei that s_j may belong to. The main constraint is to enforce assigning a boundary segment in one and only one nucleus and sharing a crease segment between two different nuclei or not using this segment at all for any nucleus. According to this consistence criterion, a "path" in $\mathcal{M}$ is defined as a routine from left to right with the so-called "boundary part" and "crease part". The boundary part passes one and only one "1" for each boundary segment column. For each pair of crease segment columns s_{n_b+2j-1} and s_{n_b+2j} which are correspondent to the same crease segment, the crease part passes either one "1" in each column but different rows or does not pass any "1" at all. Thus, each path is a segmentation of the clump with the correspondent assignments of Φ_i. In the path, every boundary segment is assigned to a nucleus while some crease segments may not be used which enables us to discard the false creases. For example, path I in Fig. 7 indicates that

$$\Phi_1 = \{b_1\},$$

$$\Phi_2 = \{b_2, c_1, b_5\},$$

$$\Phi_3 = \{b_3, b_6\},$$

$$\Phi_4 = \{b_4\},$$

$$\Phi_5 = \{c_1\},$$

$$\Phi_6 = \phi, \tag{9}$$

$\Phi_i, i = 1, 2 \ldots$ are then fitted by hyperquadrics each of which is evaluated by the criteria proposed in the next section. Thus, the nuclei segmentation problem is equivalent to finding a best path with minimum cost. For example, the best path for Fig. 6 is *Path II* as shown in Fig. 7, i.e.,

$$\Phi_1 = \{b_1, c_1, b_4\},$$

$$\Phi_2 = \{b_2, c_1, b_5\},$$

$$\Phi_3 = \{b_3, b_6\},$$

$$\Phi_4 = \phi,$$

$$\Phi_5 = \phi,$$

$$\Phi_6 = \phi. \tag{10}$$

The actual search process is based on dynamic programming [19,20], where the local cost function is defined in the next section. The dynamic programming

algorithm is essentially a multi-stage optimization technique where at each stage, or each iteration, the size of the path is increased by one set of feature segments. This process is repeated for each starting point in the assignment matrix, and the path with least cost is selected as final hypothesis.

3.3. Evaluation criteria

Although nuclei may have completely different morphology, we have some general information about their shapes and properties. This information enables us to compare different hyperquadrics, get rid of the undesirable ones, and reduce false alarms. The "goodness" criterion includes four terms: area A, shape S, overlap O and error C. Each is evaluated by its representative function E_A, E_S, E_O and E_C. The cost of the local hyperquadric is then given by $E_T = E_A + E_S + E_O + E_C$. The cost of one path is the summation of costs of the entire set of hypotheses. The transition cost between two adjacent hypotheses is simply an exclusive consistency measure. E_A, E_S, E_O and E_C are computed as follows:

1. E_A. A is the area of the hyperquadric. A nucleus should neither be bigger than (A_b) nor smaller than (A_s).

$$E_A = \begin{cases} 0, & \text{if } A_s \leqslant A \leqslant A_b, \\ 1 - e^{-(A - A_b)/\sigma_A} & \text{if } A > A_b, \\ 1 - e^{-(A_s - A)/\sigma_A} & \text{if } A < A_s, \end{cases} \tag{11}$$

where we choose $A_b = L^2$, $A_s = \frac{1}{4} L^2$.

2. E_S. S defined as an aspect ratio as measured by the ratio of minor to major axes as shown in Fig. 8(a). E_S is defined to favor perfect circles:

$$E_S = 1 - e^{-(1 - S)/\sigma_S}. \tag{12}$$

3. E_O. A hyperquadric may not always be enclosed by the nuclei clump. An overlap measure is defined as the ratio of area inside the clump to the total area of the hyperquadric. E_O is defined to favor larger values of O as shown in Fig. 8(b):

$$E_O = 1 - e^{-(1 - O)/\sigma_O}. \tag{13}$$

4. E_C. The error C is defined as $C = \varepsilon^2/m$, where ε is the error in Eq. (5) of the hyperquadric fitting process and m is the total number of points:

$$E_C = 1 - e^{-C/\sigma_C} \tag{14}$$

where $\sigma_A, \sigma_S, \sigma_O, \sigma_C$ are weighting factors for each criterion.

3.4. Post-processing

Two kinds of errors may occur in the fitting process. These include a fit that spans outside of the clumped boundary (background inclusion) and one that encloses other nuclei as well. The first problem is solved through a simple "AND" operation.

The second type of error could be either due to representation of the same nucleus with two different hyperquadric or a simple overlap between representation of two separate nuclei, as shown in Fig. 9. The first case can be easily resolved through a test in the proximity in the

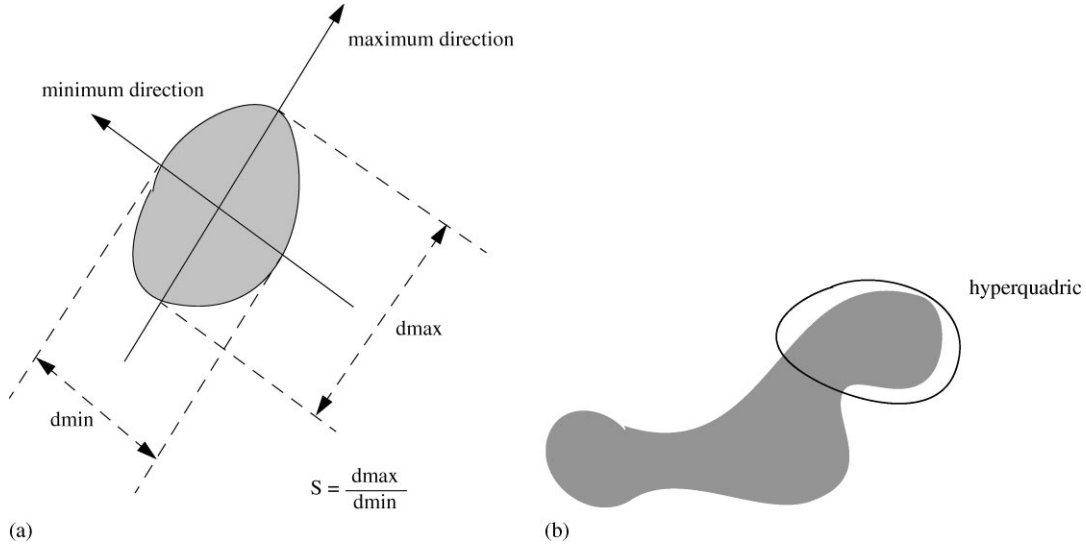

Fig. 8. Evaluation criteria. (a) Shape rate; (b) Overlap rate.

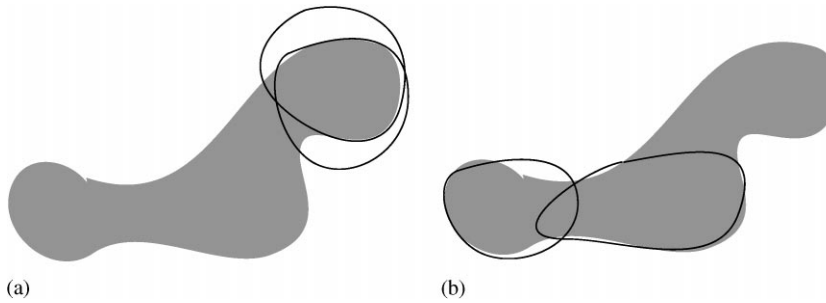

Fig. 9. Different types of error in the fit: (a) same nucleus is represented by two objects and part of background; and (b) overlap between two representations of nuclei.

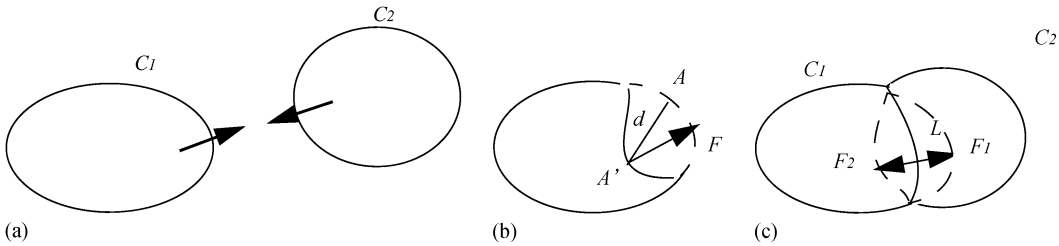

Fig. 10. Contour dynamic: (a) Two contours are squeezed together; (b) Contour dynamic; (c) Stable state.

center of mass. The second case uses a simple model to express dynamic behavior of the boundary as shown in Fig. 10(a). Let two elastic contours $\mathscr{C}_1$, $\mathscr{C}_2$ be squeezed against each other. The stable boundary between them will be affected by the rebound force that corresponds to the energy of deformation. The rebound force $\mathscr{F}$ at any point on the deformed contour is proportional to its displacement d from the original position and perpendicular to the new boundary, as shown in Fig. 10(b), $\mathscr{F} = \alpha d$. And the deformation energy is given by $e = \int_{L2} \frac{1}{2}\beta d^2 \, ds$, where α, β are elastic parameters. At equilibrium, $\mathscr{F}_1 = \mathscr{F}_2$ along L and the deformation energy should be minimum, as shown in Fig. 10(c). Then it is not difficult to prove that every point on L must have the same distance from its original positions on $\mathscr{C}_1$ and $\mathscr{C}_2$.

Hence, we use a protocol based on distance transform to partition squeezed hyperquadrics. Let region $\mathscr{R}$ contain h hyperquadrics h_i, $i = 1, \ldots, h$ with some overlap where the distance transformations, $\mathscr{D}_i(x, y)$, for each hyperquadric is computed. Then each point $(x, y) \in \mathscr{R}$ is assigned to ith nucleus if $\mathscr{D}_i(x, y) \geqslant \mathscr{D}_j(x, y)$, $\forall j = 1, \ldots, h$ as shown in Fig. 11(a) and (b).

3.5. Experimental results and discussions

The proposed protocol has been tested on real data obtained from a fluorescence microscope. The results computed by our approach as well as the "correct" segmentations generated manually by skilled operator interaction are presented in Figs. 12–16. Comparisons between the two types of results are summarized in the following Table 1.

"Manual" column presents the numbers of nuclei detected by the skilled operator and those in "Algorithm" are numbers of nuclei detected by our algorithm. "Rejected" are the differences between the proceeded columns.

Analysis of the output of our algorithm is given in Table 2.

"Bad location" indicates the numbers of nuclei with incorrect partial boundary locations; "Fused" are the numbers of nuclei that are fused to other ones; "Fragmented", the numbers of nuclei that are fragmented into two or more small shapes. The "Acceptable" column gives us the numbers of nuclei correctly detected by our algorithm and "Reliability" are the percentages of acceptable nuclei to all detected ones.

As we can see, the nuclei lying on the boundaries of the original images are rejected since most of their boundary segments cannot be provided. In Fig. 15, one nucleus is fragmented into two small shape because of the false crease information. The absence of crease segment as well as the fact that, in some situations, a bigger nucleus is "better" than two very small ones according to our criteria, leads to the fusion of nuclei in Figs. 15 and 16. "Bad location" happens in Figs. 12 and 13 and 16 because the boundary information is not strong enough to enhance

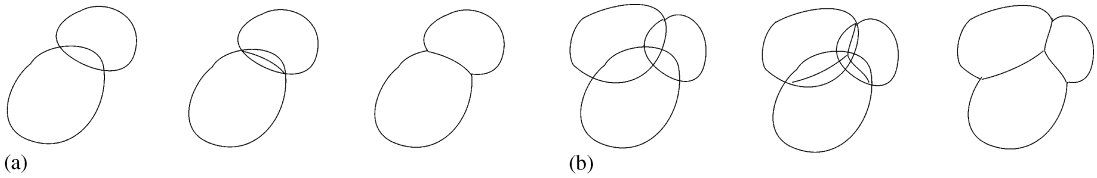

Fig. 11. Steps in resolving the overlap problem between multiple nuclei: (a) two nuclei; (b) three nuclei.

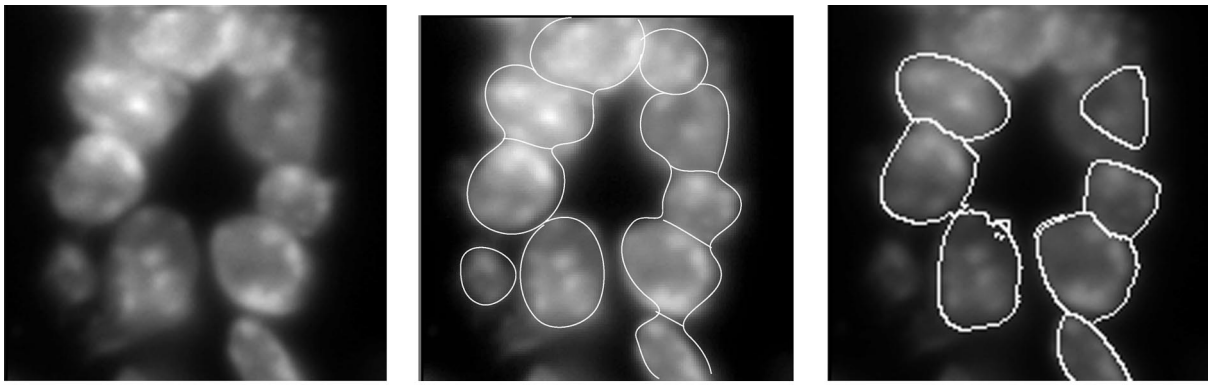

Fig. 12. Segmentation results: (a) original image; (b) correct segmentation; (c) our segmented nuclei.

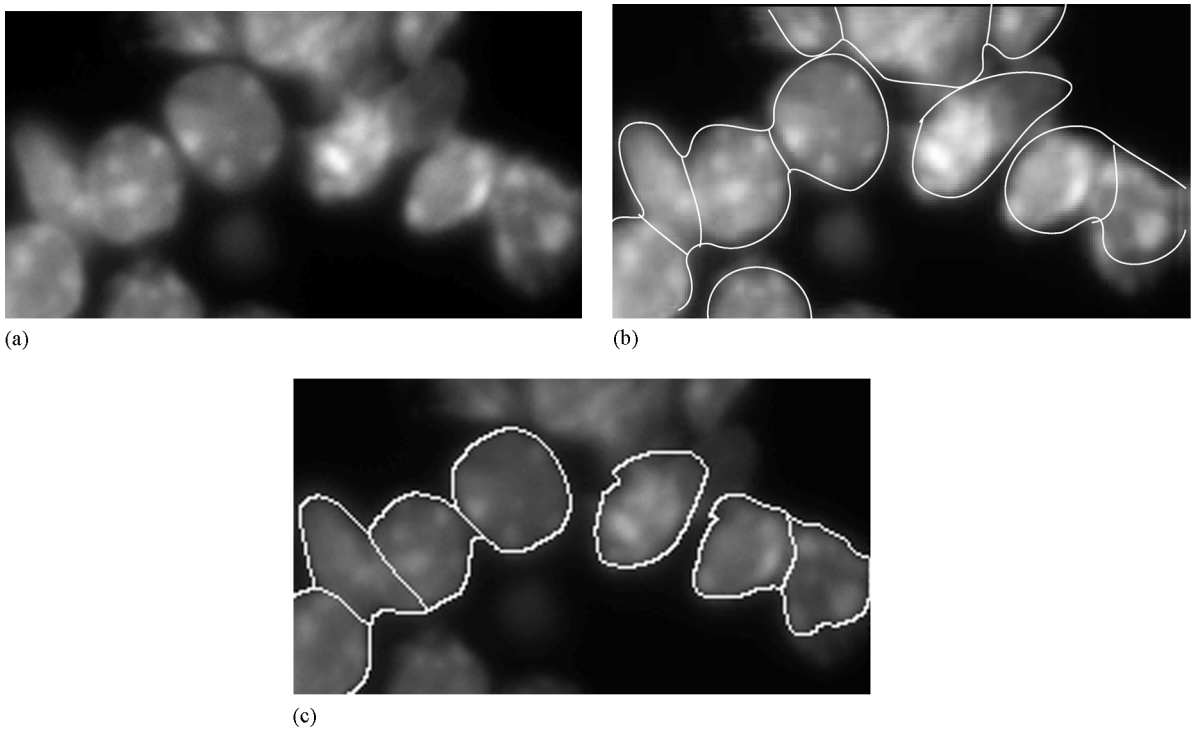

Fig. 13. Segmentation results: (a) original image; (b) correct segmentation; (c) our segmented nuclei.

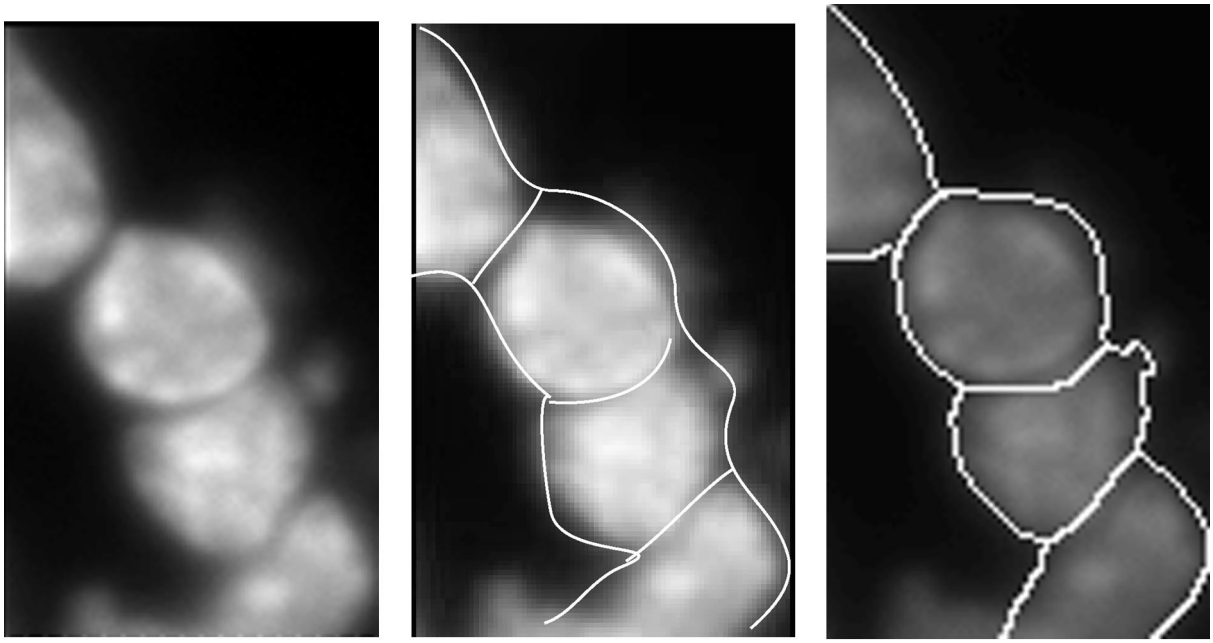

(a) (b) (c)

Fig. 14. Segmentation results: (a) original image; (b) correct segmentation; (c) our segmented nuclei.

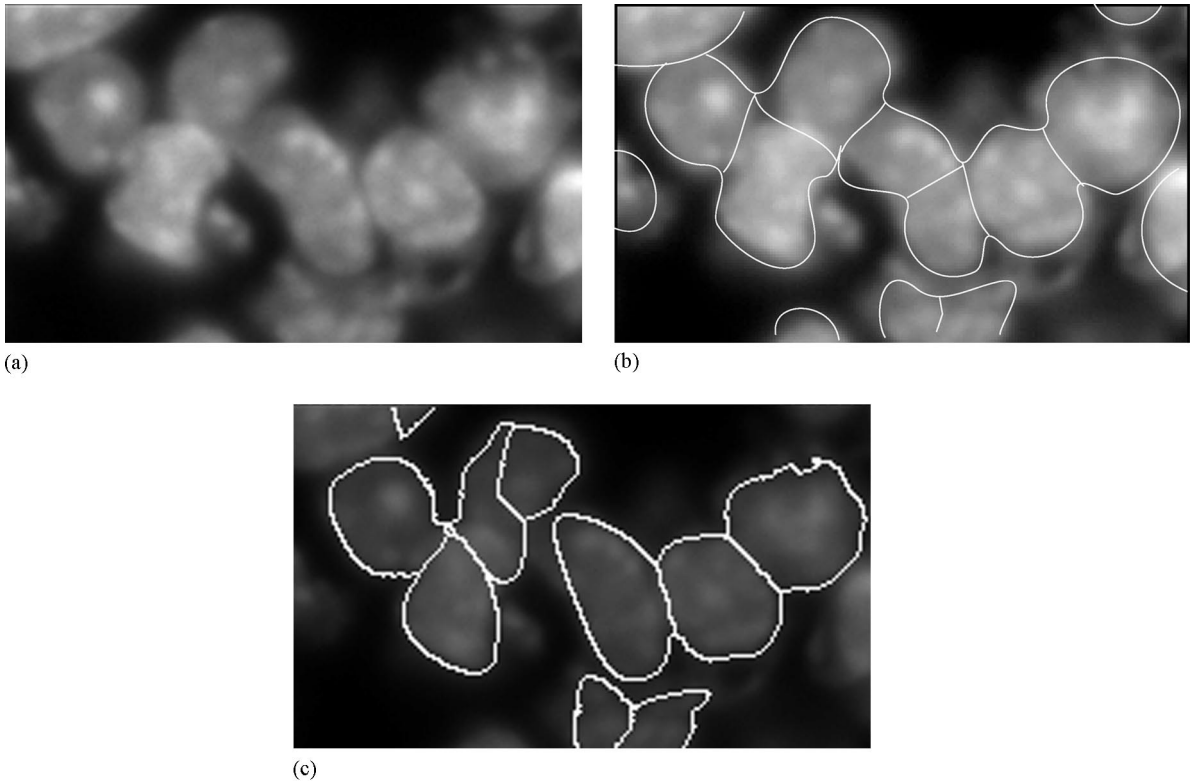

(a) (b)

(c)

Fig. 15. Segmentation results: (a) original image; (b) correct segmentation; (c) our segmented nuclei.

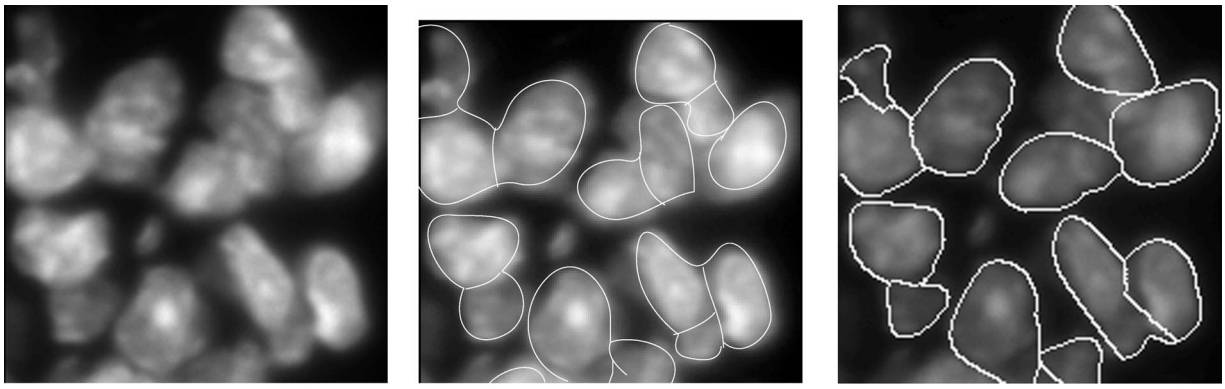

(a) (b) (c)

Fig. 16. Segmentation results: (a) original image; (b) correct segmentation; (c) our segmented nuclei.

Table 1
Numbers of nuclei detected by the two methods

Figure index	Manual	Algorithm	Rejected
12	10	7	3
13	11	7	4
14	4	4	0
15	12	9	3
16	14	12	2

the concavity. Since our approach seeks a global solution, it is possible that some local incorrect segmentations be the cost for a better global optimization.

In all of the experiments, the hyperquadric has four terms, $N = 4$. The evaluation parameters are $L = 45$, $\sigma_A = 200$, $\sigma_S = 5$, $\sigma_O = 0.5$ and $\sigma_C = 1$. These numbers are obtained based on a priori information in the specific application domain.

4. Conclusion

We have presented a new approach for segmentation of nuclei based on partial geometric information. Two key issues are hyperquadric fitting and assignment matrix. Hyperquadric representation can model a broad range of shapes from partial boundary information. The assignment matrix, on the other hand, converts the segmentation problem into a constrained optimization problem. Our approach aims for global consistency, and as a result, it is less error prone and generates a few false alarm for final verification by an operator.

Acknowledgements

Authors thank Dr. Mary Helen Barcellos-Hoff and Mr. Sylvain Costes for motivating the problems, valuable discussion, and providing the data used in this experiment. This work is supported by the Director, Office of Energy Research, Office of Computation and Technology Research, Mathematical, Information, and Computational Sciences Division, and Office of Biological and Environmental Research of the U. S. Department of Energy under contract No. DE-AC03-76SF00098 with the University of California. The LBNL publication number is 643205.

References

[1] M. Sonka, V. Hlavac, R. Boyle, Image Processing Analysis and Machine Vision, Chapman & Hall, London, 1995.

Table 2
Detailed analysis of our results

Figure index	Bad location	Fused	Fragmented	Acceptable	Reliability (%)
12	1	0	0	6	88
13	1	0	0	6	88
14	0	0	0	4	100
15	0	1	1	7	77
16	1	1	0	10	83

[2] H. Talbot, I. Villalobos, Binary image segmentation using weighted skeletons, SPIE Image Algebra Morphol. Image Process. 1769 (1992) 393–403.
[3] J. Leu, H. Yau, Detection of the dislocations in metal crystals from microscopic images, Pattern Recognition 24 (1) (1991) 41–56.
[4] S. Ong, H. Yeow, R. Sinniah, Decomposition of digital clumps into convex parts by contour tracing and labelling, Pattern Recognition Lett. 13 (1992) 789–795.
[5] J. Liang, Intelligent splitting the chromosome domain, Pattern Recognition 22 (1989) 519–532.
[6] Y. Jin, Jayasooriah, R. Sinniah, Clump splitting through concavity analysis, Pattern Recognition 15 (1994) 1013–1018.
[7] W. Wang, Binary image segmentation of aggregates based on polygonal approximation and classification of concavities, Pattern Recognition 31 (10) (1998) 1502–1524.
[8] O. Monga, N. Ayache, P. Sander, From voxel to intrinsic surface features, Image Vision Comput. 10 (6) (1992).
[9] O. Monga, S. Benayoun, O. Faugeras, From partial derivatives of 3D density images to ridge lines, Proceedings of the Conference on Computer Vision and Pattern Recognition, 1992, pp. 354–359.
[10] J. Thirion, A. Gourdon, The 3D matching lines algorithm, Graph. Model Image Process. 58 (6) (1996) 503–509.
[11] J. Thirion, New feature points based on geometric invariants for 3D image registration, Int. J. Comput. Vision 18 (2) (1996) 121–137.
[12] R. Gonzalez, R. Woods, Digital Image Processing, Addison-Wesley, Reading, MA, 1992.
[13] P. Saint-Marc, J. Chen, G. Medioni, Adaptive smoothing: A general tool for early vision, IEEE Trans. Pattern Anal. Mach. Intell. 13 (6) (1991) 514–530.
[14] D. Struik, Lectures on Classical Differential Geometry, Dover Publications, New York, 1988.
[15] S. Han, D. Goldgof, K. Bowyer, Using hyperquadric for shape recovery from range data, Proceedings of the IEEE International Conference on Computer Vision, 1993, pp. 292–296.
[16] A. Hanson, Hyperquadrics: smoothly deformable shapes with convex polyhedral bounds, Comput. Vision, Graphics, Image Process. 44 (1988) 191–210.
[17] S. Kumar, S. Han, D. Goldgof, K. Boeyer, On recovering hyperquadrics from range data, IEEE Trans. Pattern Anal. Mach. Intell. 17 (11) (1995) 1079–1803.
[18] W. Press, S. Teukollsky, W. Vetterling, B. Flannery, Numerical Recipes in C, Cambridge Uni. Press, Cambridge, England, 1992.
[19] B. Parvin, C, Peng, W. Johnston, M. Maestre, Tracking of tubular molecules for scientific applications, IEEE Trans. Pattern Anal. Mach. Intell. 17 (1995) 800–805.
[20] R. Bellman, Dynamic Programming, Princeton University Press, Princeton, NJ, 1957.

About the Author—GE CONG received the BS degree in electrical engineering from Wuhan University, Wuhan, China in 1992 and the Ph.D degree in computer science from Institute of Automation, Chinese Academy of Sciences in 1997. He is currently a staff scientist in Lawrence Berkeley National Laboratory. His research interests include computer vision, pattern recognition and bioinformatics.

About the Author—BAHRAM PARVIN received his Ph.D. in Electrical Engineering from University of Southern California in 1991. Since then he has been on the staff at the Information and Computing Sciences Division at Lawrence Berkeley National Laboratory. His areas of research include computer vision and collaboratory research. He is a senior member of IEEE.